Compression characteristics and fractography of in-situ polymerisable thermoplastic and bio-epoxy based non-crimp carbon and glass fibre composites

Gursahib Singh Bhatia[1], Kieran Fahey[1], Akshay Hejjaji[1], Jayaram Pothnis[1] and Anthony Comer[1*]

[1]Bernal Institute (Composites), School of Engineering, University of Limerick, Ireland

Corresponding author: Anthony Comer
Email address: Anthony.Comer@ul.ie

Abstract

This experimental work involves characterization and fractography of a bio-based epoxy and an in-situ polymerisable thermoplastic polymer matrix based non-crimp glass and carbon fibre composites under compressive loading. The laminates are characterized under compression loading using a combined loading compression (CLC) fixture. Laminates made using the thermoplastic matrix exhibit higher compressive strength (approx. 20% along fibre direction) compared to the bio-epoxy based laminates. Further, both composites exhibit comparable compressive modulus characteristics. The tested composites are subjected to fractography analysis using Scanning Electron Microscopy (SEM) and Computed tomography (CT). SEM results indicate a difference in fibre-matrix interface characteristics between the thermoplastic matrix and the bio-epoxy matrix. Additionally, the CT scans reveal a difference in failure modes due to fibre orientations. A difference between failure mode of the exterior and interior plies of the specimens was also noticed. However, no specific influence of matrix type was observed on the overall macroscopic failure behavior.

Keywords: Infusible Thermoplastic, Bio-Epoxy, Compression, Fractography, Experimental Characterization

Highlights:

- Bio-epoxy and thermoplastic based laminates were characterized in compression.
- Post-test fractography was performed using SEM and X-ray CT scans.
- Use of thermoplastic matrix exhibits better fiber-matrix adhesion compared to bio-epoxy.
- Both laminates performed well in compression under laboratory test conditions.

1. Introduction

In recent times, there has been a significant increase in the installation and commissioning of offshore wind energy structures globally. This trend is expected to continue in the future as nations attempt to reduce carbon emissions associated with energy production [1–3]. Steel is generally employed as the primary material in offshore energy structures such as floating wind turbine platforms consisting primarily of one or more towers and a floating substructure. However, the sea environment renders steel structures susceptible to corrosion [4]. One of the most promising solutions to this problem is to re-design and replace steel structures with structures manufactured using fibre reinforced polymers (FRPs)[5]. FRP materials are immune to metallic corrosion and are generally superior in terms of their fatigue performance [6]. With an increase in the scale of offshore energy projects, the usage of FRPs is expected to increase significantly. This can result in a concurrent increase in environmental impact in terms of the synthesis, manufacture, maintenance, and end-of-life disposal of FRP structures [7,8].

Conventional FRP materials comprising petroleum-based thermosetting epoxy matrix composites pose serious environmental concerns at the end-of- life stage due to challenges in recovery and/or disposal[9]. Various efforts are being made globally to reduce

the environmental impact of FRPs both at source and at end-of-life (EOL) stage. One promising option is to replace petroleum-based epoxies with bio-epoxies (derived from bio sources). The bio-based epoxies contain compounds which are partially sourced from plant sources, thus making them a relatively sustainable alternative to petroleum-based epoxies. Another promising option is to use thermoplastics due to their potential recyclability at EOL stage [10,11]. However, use of bio-epoxies and thermoplastics to realize large offshore structures is based on their suitability to be processed using existing manufacturing techniques in the industry such as vacuum resin infusion with in-situ polymerisation and low temperature post cure. Further it is essential that their properties are comprehensively characterized with an established understanding of the failure mechanisms during mechanical loading. A literature review by the authors specifically on commercially available infusible in-situ polymerizable thermoplastics and bio epoxy based composites which are suitable for vacuum infusion process with low temperature post cure, reveals that very limited mechanical characterization data is available. A summary of the key studies available in literature is presented in the following paragraphs.

Haggui *et al.* characterized flax fibre laminates made with an in-situ polymerizable thermoplastic under both static and fatigue (tensile) loading conditions [12]. Using acoustic emission (AE) technique during testing, the authors identified different damage mechanisms such as matrix micro-cracking, fibre-matrix debonding, fibre-pull out and, fibre-breakage and the S-N curves of the tested laminates was presented in the study. Barbosa *et al.* characterised the out-of-plane properties of in-situ polymerizable thermoplastic-carbon fibre laminates and compared them with epoxy-based laminates [13]. They reported thermoplastic based laminates to offer higher resistance to Mode II

interlaminar fracture as compared to epoxy-based laminates. In another study, Kazemi *et al.* characterized the mechanical properties under different loading configurations for laminates with plain weave ultra-high molecular weight polyethylene fibres, plain weave carbon fibres and their hybrid layups [14]. They reported that the Young's modulus and tensile strength of carbon/thermoplastic laminates was very similar to that of carbon/epoxy laminates manufactured in the same study. The result highlights the competitiveness of in-situ polymerizable thermoplastic resin with respect to epoxy resin. Pini *et al.* investigated interlaminar fracture behaviour of carbon fibre laminates prepared using plain and toughened in-situ polymerizable thermoplastic resin[15,16]. They observed an improved fibre-matrix adhesion with the toughened thermoplastic. Obande *et al.* characterized the mechanical (tensile, flexural, short beam shear and mode-I fracture toughness) and thermomechanical response of non-crimp glass fibre reinforced thermoplastic laminates and benchmarked them against epoxy-based laminates [17]. Superior tensile (90°), flexural (0°), interlaminar-shear and fracture toughness properties were reported for the thermoplastic based laminates. Nash *et al*. investigated the effects of environmental conditioning on the mechanical and thermomechanical properties of in-situ polymerizable thermoplastic based laminates and laminates manufactured using commonly used matrix systems for marine applications[18]. They reported comparable material properties for the laminates with thermoplastic with the epoxy-based laminates under dry conditions. However, a reduction of interlaminar shear strength for thermoplastic based composites in wet (immersed under deionised water) conditions was attributed to the transition of failure from being matrix dominant in dry state to fibre-matrix interfacial in wet state, indicating the need of fibre sizing specifically compatible with the acrylic-based resin systems. Jia

and Fiedler investigated the tensile creep behaviour of bio-epoxy based laminates reinforced with unidirectional flax fibres [19]. For offshore structural applications however, flax based laminates exhibit some limitations as studies have shown that flax-based laminates experience a degradation in their mechanical performance when exposed to moisture[20–22]. There are other characterization studies reported in literature with different bio-epoxies, however those resins are not suitable candidate for offshore energy sector due to manufacturing limitations. Hence those works are not discussed here.[26]

Overall, from literature, it is seen that very limited studies have characterized the properties of infusible in-situ polymerizable thermoplastics and bio epoxy-based composites under mechanical loadings. Further, majority of the reported studies employ woven or multiaxial fabrics. However, ply-level material data from unidirectional composites is primarily required for numerical models. Further, an understanding of the compressive response of non-crimp unidirectional fibre reinforced laminates considering a Bioepoxy and an in-situ polymerizable thermoplastic is lacking.

Hence, in this work an experimental investigation is carried out to study the compressive response of FRP composites employing an in-situ polymerizable thermoplastic and a bio-epoxy as matrix materials for two non-crimp unidirectional reinforcements comprised of carbon fibres (CF) and glass fibres (GF) keeping their suitability under offshore environment in mind. For all four resin-fibre combinations (GF/ Thermoplastic, GF/ Bio-epoxy, CF/ Thermoplastic, CF/Bio-epoxy), the testing is performed in both the longitudinal ($[0°]_n$) and transverse ($[90°]_n$) loading directions with respect to the fibre orientation. Thereafter, the representative tested specimens are subjected to inspection under scanning electron microscopy (SEM) and computed

tomography (CT) scans to identify the characteristic failure mechanisms observed for both the matrix types.

2. Experimental Details

2.1. Materials and Manufacturing

The required laminates were prepared using an in-situ polymerizable acrylic based thermoplastic resin (trade name- Elium®) and a bio-epoxy (trade name- InfuGreen®) as matrix materials. Elium was chosen as the thermoplastic, as this resin has shown a potential to manufacture large structures using vacuum infusion process as demonstrated in the project ZEBRA [23]. Generally, melt processable thermoplastics require processing at elevated temperatures (typically well above 100 °C) which makes them unsuitable for existing large scale manufacturing facilities using vacuum infusion, which are primarily designed for manufacturing of epoxy based laminates with cure temperature up to 60°C. However, acrylic based Elium is the only thermoplastic currently commercially available which is infusible at room temperature and requires post processing at temperatures under 60 °C. Hence the acrylic based Elium was chosen as the required matrix material. For bio-epoxy, Terry *et al*. provided a comparison of nine commercially available bio-based neat resin systems [24]. From the comparison, it is inferred that InfuGreen® 810 is one of the most viable bio-epoxy options for offshore structures using the vacuum assisted liquid resin infusion technique. The technical specifications of both resin systems used are summarised in Table 1. Two non-crimp fabrics comprising of glass fibre (GF) and carbon fibres (CF) with areal density 1182 g/m^2 and 438 g/m^2 respectively, were employed as reinforcements. A schematic representing the fabric architecture of both glass fabric and carbon fabric is depicted in Fig. 1(c). The glass fabric is made up of 96% of the primary glass fibres distributed along the warp direction and 3% of the secondary glass fibres distributed along

the weft direction. The carbon fabric constitutes over 93% of the primary carbon fibres along the warp direction and 3.6% of glass fibres incorporated at ±60° to the warp direction. In addition to the primary and secondary fibres, polyester yarn (amounting for ≈ 1 % in Glass fabric and ≈ 2-3 % in carbon fabric) is used for stitching. The secondary fibres and the polyester stitching stabilize the fabric and aid in handling and storage. The laminates employing thermoplastic (Elium®) were prepared using two different grades viz. Elium® 188XO for glass fabric and Elium® 188O for carbon fabric, as recommended in the technical datasheets for Elium® 188[25,26]. The laminates were prepared using the vacuum assisted liquid resin infusion technique and cured initially at room temperature. Samples of width 13 mm and length 140 mm as per ASTM D6641[27], were extracted from the cured laminates using abrasive waterjet cutting technique. The extracted test specimens were heated at 60°C for 24 hrs and at 60°C for 16 hrs for the thermoplastic and bio epoxy-based laminates respectively as per the polymerisation cycles described in corresponding technical datasheets (TDS). Table 2 lists all the layups tested in this experimental campaign. In total, 8 material combinations were tested considering fibre dominant ($[0]_n$) and matrix dominant ($[90]_n$) layup configurations. The fibre volume fraction (FVF) was determined using the thickness measurement method as per ISO 14127 standard. Equation 1 was used to calculate the fibre volume fraction. The thickness of each of the specimen was measured at four different locations and the average thickness was used to calculate the volume fraction of fibres in each specimen. Thereafter, an overall volume fraction was computed for each laminate type (viz. GF/Elium, GF/InfuGreen, CF/Elium and CF/InfuGreen) considering the average of the volume fractions of all specimens within that laminate type. The fibre volume fraction measurements for GF InfuGreen laminates were

performed using Burn-off tests to validate the FVF obtained through thickness measurement tests. The resulting FVF using burn-off test was very close to the FVF obtained using thickness measurement as per ISO 14127 standard. For reference, the average FVF obtained from Burn-off method was 59.04 while the average FVF from the thickness measurement method was 58.71. The difference was very marginal. Hence, the void content was assumed to be negligible which was again confirmed through SEM and X-Ray Tomography cross sectional images. The fibre volume fraction was reported using thickness measurement method as per ISO 14127.

$$FVF\ (\%) = \frac{Number\ of\ plies \times mass\ per\ unit\ area\ of\ fabric\ (\frac{g}{m^2})}{thickness\ (mm) \times fibre\ density\ (\frac{g}{cm^3})} \times 10^{-1} \quad (1)$$

Table 1 Resin systems used for manufacturing and the processing parameters according to manufacturer datasheets.

	Thermoplastic Acrylic (Arkema)		**Thermosetting Bioepoxy (Sicomin)**
Name	Elium® 188XO (for glass fibres)	Elium® 188O (for carbon fibres)	SR InfuGreen® 810
Curing Agent	Perkadox GB-50X (Powder)	Perkadox GB-50X (Powder)	SD8824 (Liquid)
Mass Ratio (Resin : Curing Agent)	100 : 3	100:3	100 : 22
Viscosity	100 mPa.s @25°C	100 mPa.s @25°C	120-320 mPa.s @25°C
Curing time at ambient	24 hr	24 hr	24 hr
Post-infusion heating/processing temperature	60 °C	60°C	60 °C
Post-infusion heating time	24 h	24h	16 h
Storage Life	6 months	6 months	24 months
Tensile Strength	56 MPa	56 MPa	65 MPa
Tensile Modulus	2.6 GPa	2.6 GPa	2.8 GPa

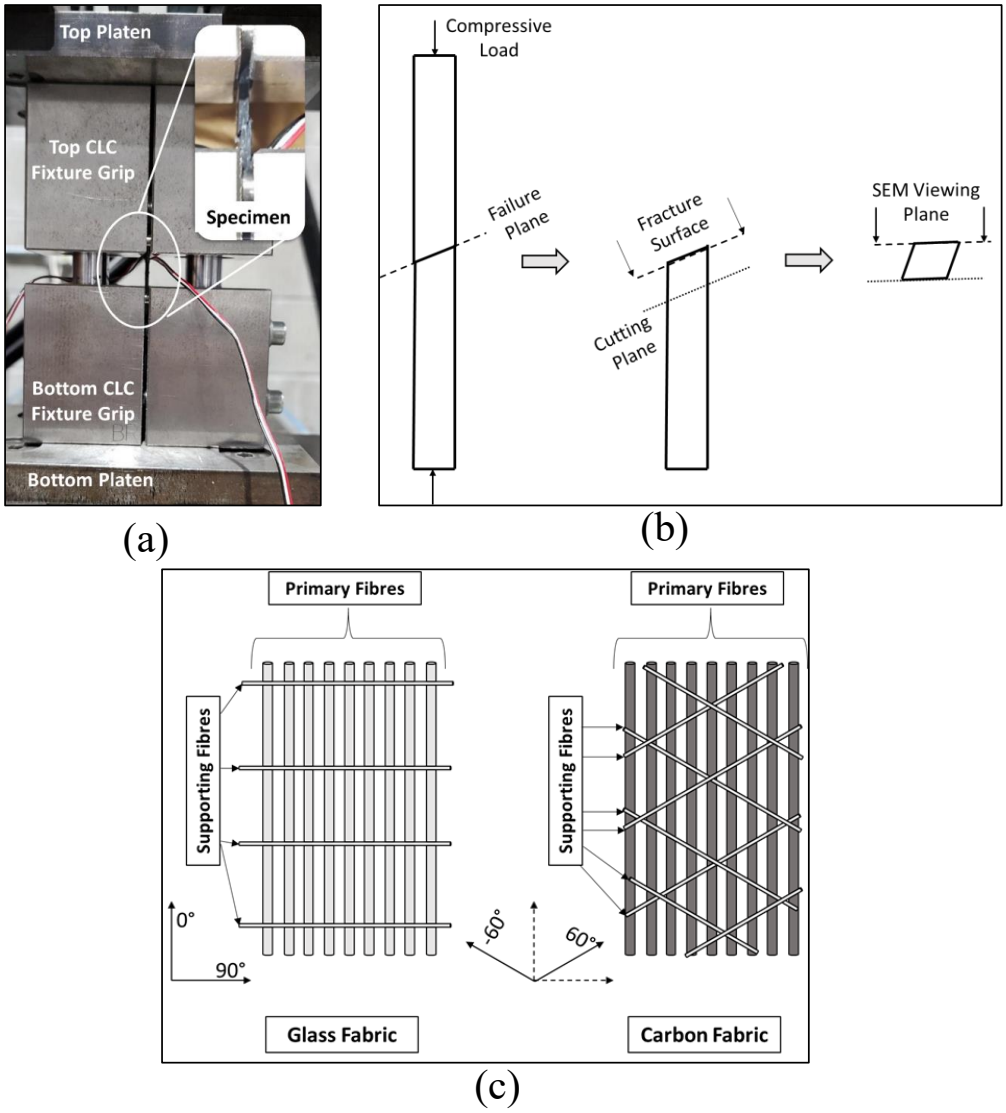

Fig. 1. (a) The CLC test fixture showing a representative specimen under testing (b) Schematic representation of specimen preparation for SEM (c) Schematic representation of fabric structure (not to scale) depicting arrangement of primary (load bearing) and secondary (supporting) fibres

Table 2 Laminate constituents and lay-ups for vacuum assisted liquid resin infusion.

Reinforcement	Lay-up	Resin	Initiator
Glass Fabric (GF) Saertex U-E 1182 g/m2 Primary 0° fibres: NEG Hybon 2026 E-glass fibre 1134 gsm Supporting fibres: 90° NEG Hybon 2026 E-glass fibre 36 gsm	$[0]_{2S}$	Elium® 188 XO	Perkadox GB-50X
	$[90]_{2S}$	Elium® 188 XO	
	$[0]_{2S}$	SR InfuGreen® 810	SD8824

Overall Areal weight: 1182 gsm Stitching: PES 12 gsm Sizing: Silane	$[90]_{2S}$	SR InfuGreen® 810	
Carbon Fabric (CF) Saertex U-C 438 g/m2 Warp: Mitsubishi Pyrofil TR50S 1.2k Carbon fibre, 410 gsm Supporting fibres: ±60° E-glass fibre 16 gsm Overall Areal weight: 438 gsm Stitching: PES 12 gsm Sizing: Proprietary Organic Sizing	$[0]_{4S}$	Elium® 188 O	Perkadox GB-50X
	$[90]_{2S}$	Elium® 188 O	
	$[0]_{4S}$	SR InfuGreen® 810	SD8824
	$[90]_{4S}$	SR InfuGreen® 810	

2.2. Compressive Test Procedure

Compression testing was performed using a Combined loading compression (CLC) test fixture as per ASTM D6641[27]. Fig. 1 (a) displays the test setup employed. The tests were conducted under displacement control mode with a crosshead displacement rate of 1.3 mm/min. A gage length of 13 mm was maintained as per test standard. Two strain gages were bonded on to each of the specimens, one on each face of the individual specimen. The modulus (for both 0° and 90° specimens) was calculated as the chord modulus over a strain range of 0.001- 0.003. The tests were stopped after a sudden drop in load was observed. The tested specimens were then inspected to validate conformity of the failure mode as per ASTM D6641[27]. The data from at least three valid specimens was taken for modulus calculations in each test case. The standard deviation along with the characterized properties are reported in Table 3.

Table 3 Tabulated summary of characterized properties

Lay-up	Properties	Determined Properties			
		GF/Thermoplastic	**GF/Bio-epoxy**	**CF/Thermoplastic**	**CF/Bio-epoxy**
0°	σ_{11}^{max} (MPa)	676.0 [612.5*] (96.8)	529.2 [495.7*] (29.5)	577.9 [649.5*] (42.8)	488.1 [539.5*] (100.2)
	σ_{11}^{f} (MPa)	670.3 [607.4*] (94.4)	527.0 [493.7*] (33.3)	553.9 [622.5*] (42.3)	483.4 [534.3*] (104.9)
	E_{11} (GPa)	46.6 [42.2^] (3.3)	45.3 [42.4^] (0.7)	96.6 [108.6^] (2.9)	98.3 [108.6^] (10.8)
	V_f (%)	60.70	58.71	48.94	49.76
90°	σ_{22}^{max} (MPa)	149.0 (10.8)	142.6 (4.5)	133.0 (5.6)	119.8 (2.7)
	σ_{22}^{f} (MPa)	145.9 (10.7)	136.0 (8.1)	132.3 (4.8)	118.9 (3.4)
	E_{22} (GPa)	16.7 (0.7)	15.7 (0.3)	7.7 (0.3)	7.4 (0.2)

Note- GF: Glass Fibre, CF: Carbon Fibre; σ_{11}^{max}= Maximum compressive strength in fibre direction, σ_{11}^{f}= Compressive strength at failure in fibre direction, E_{11} = Modulus in fibre direction, σ_{22}^{max}= Maximum compressive strength transverse to fibre direction, σ_{22}^{f}= Compressive strength at failure transverse to fibre direction, E_{22} = Modulus transverse to fibre direction, V_f = Fibre volume fraction, Failure is defined here as the instance during the test where first significant drop in load is observed, the specimen may still be bearing the load beyond failure initiation and reach a peak value. Standard deviation values in round parenthesis; Normalized values in square brackets. *Normalized Strength =Strength × 0.55/Absolute V_f; ^Normalized Modulus=Modulus × 0.55/Absolute Vf

2.3. Failure Analysis and Fractography Procedure

Failed samples were subjected to visual inspection prior to select specimens undergoing computed tomography (CT) scans. Fractography observations were made using scanning electron microscopy (SEM). The procedure for both the techniques is outlined below.

2.3.1. Computed Tomography (CT)

To investigate the variation in damage characteristics with respect to location within the specimens, a cross-sectional inspection was conducted using the computed tomography

scans (CT) along both longitudinal and transverse directions with respect to the loading axis. Representative GF specimens were scanned under computed tomography (CT). After a careful visual inspection of the tested GF specimens, one specimen representing typical failure observed under each of the four test cases (viz. (i) GF/Thermoplastic 0° (ii) GF/Thermoplastic 90° (iii) GF/Bio-epoxy 0° (iv) GF/Bio-epoxy 90°) was selected for CT scans. While extracting the CT specimen section from the tested CLC specimens, a length of 5 mm on either side of the fracture plane was considered as the length of CT scan specimen. The total length was approx. 10 mm and the width, thickness were retained as in the original CLC specimen. The specimen extraction procedure was performed very carefully using a precision cutter without disturbing the failed region of the tested specimens. CT scans were performed using VTOMEX L 300 X-ray microtomography scan equipment using a voltage of 130 kV and current of 180 µA. The scans were conducted with a resolution of 8 µm.

2.3.2. **Scanning Electron Microscopy (SEM)**

A valid representative specimen from each tested layup was chosen for microscopy analysis using a Hitachi SU-70 high-resolution scanning electron microscope (SEM). The specimens were carefully selected to represent the failure mode observed in each test configuration. The overall failure mode appeared similar in all the tested specimens within each test case as shown in Fig. 4 and Fig. 5. Upon removal of tested specimen from the fixture, the specimen could be separated in two pieces about the fracture plane by applying very little force by hand, thereby exposing the fracture plane surface as shown in Fig. 1(b). A small length section was thereafter extracted from the selected specimens with a cut plane oriented parallel to the plane of the fracture as depicted in Fig. 1(b). The fracture surface was coated with gold by vacuum sputtering at 20 mA for at least 40 s before

conducting SEM analysis. Beam voltages of 5 kV and 10kV was used to obtain the SEM images without causing overcharging of the specimens. A schematic representation providing the perspective of the region analysed under SEM is depicted in Fig. 1(b).

3. Results and Discussion

3.1 Compressive Response

During compression testing, it was observed that the strain gages typically failed prior to the ultimate failure of the specimens. However, the strain data is available over the strain range (0.001- 0.003) recommended for the calculation of modulus as per ASTM D6641 as presented in Fig. 2 and Fig. 3. The characterized properties are also tabulated in Table 3. In the case of fibre dominant specimens (0° specimens), the characterized properties are normalised to 55% fibre volume fraction (V_f = 0.55). The volume fraction calculated for the 0° laminate is included in Table 3.

From Table 3, a comparison between fibre dominant 0° GF/Thermoplastic and GF/Bio-epoxy specimens reveals that the thermoplastic specimens exhibit higher compressive strength (approximately 23 % higher) compared to bio-epoxy specimens. A similar trend is also observed in the case of CF/Thermoplastic specimens (approximately 20 % higher as compared to CF/Bio-epoxy). Similarly, in the case of matrix dominant 90° specimens, the GF/Thermoplastic specimens exhibit higher strength (approximately 4.5 % higher) compared to GF/Bio-epoxy specimens. Likewise, CF/Thermoplastic specimens possess higher strength (approximately 11 % higher) when compared with CF/Bio-epoxy specimens. Thus, it can be inferred that for the same type of reinforcement, thermoplastic based laminates have higher compression strength compared to bio-epoxy based laminates. The post fracture SEM images for thermoplastic laminates (cf. Fig. 8 for GF/Thermoplastic and Fig.9 for CF/Thermoplastic) clearly reveal presence of matrix on the bare fibres after

failure indicating cohesive failure at the fiber-matrix interface. Additionally, signs of micro ductility is observed for the thermoplastic laminates (cf. Fig.9b and 9c). This indicates that thermoplastic laminates exhibit slightly ductile deformation. However, from the SEM images it is seen that bio-epoxy laminates have clean fibers post failure indicating adhesive failure at the interface. Additionally, fractured matrix surfaces indicate occurrence of sudden brittle failure. Micro ductility of thermoplastic leads to better load taking capacity along with better load transfer ability of thermoplastic interface. Hence, thermoplastic laminates clearly have higher compressive strengths compared to bio-epoxy laminates where sudden brittle failure is observed. This is true for both 0° and 90° fiber orientation cases. However, for the modulus, it is observed that the specimens of both the matrix types performed similar. The difference is not significant to indicate any definitive trend.

In the case of 90° specimens, higher modulus values are exhibited by GF-based specimens for both thermoplastic and bio-epoxy matrix when compared with the corresponding CF 90° specimens. Likewise, in terms of the strength, the CF/Thermoplastic 90° specimens performed poorer compared to GF/Thermoplastic 90° specimens. A similar trend is also observed in the case of the bio-epoxy matrix, wherein the CF/Bio-epoxy specimens exhibit lower strength compared to GF/Bio-epoxy specimens. This phenomenon is observed specifically due to the architecture of the fabrics employed in this work. In the case of GF 90° specimens, the secondary fibres (refer Fig. 1(c)) align with the loading direction, resulting in the specimen exhibiting a higher modulus and strength. However, the secondary fibres in the case of the carbon fabric are aligned at ±60°, which do not align along the loading direction and hence do not contribute significantly to the stiffness or strength. Hence due to the presence of some secondary fibres in the loading direction in

90° glass fibre specimens a higher modulus is being observed. Thus, it can be deduced that, the modulus and strength under compression for a polymer are significantly influenced by the presence of a small fraction (approx. 3%) of reinforcement.

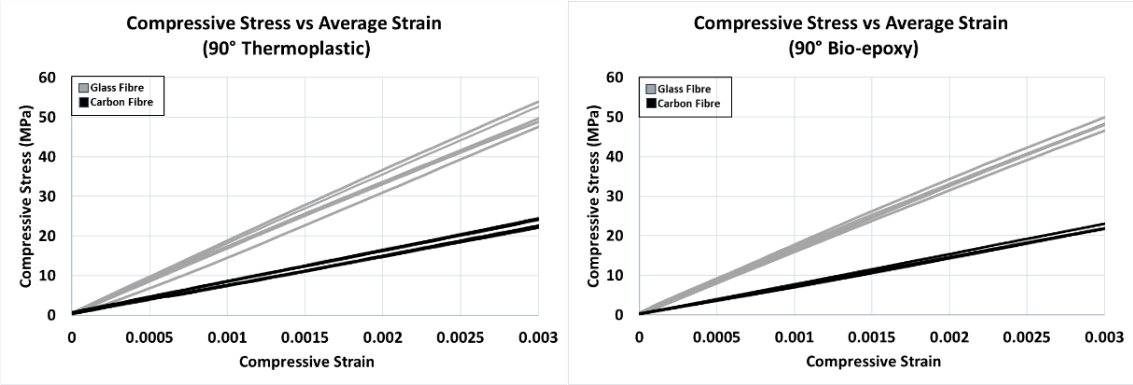

(a) (b)

Fig. 2. Stress-strain response curves for test coupons of 90° layup with (a) Thermoplastic (b) Bio-epoxy resin.

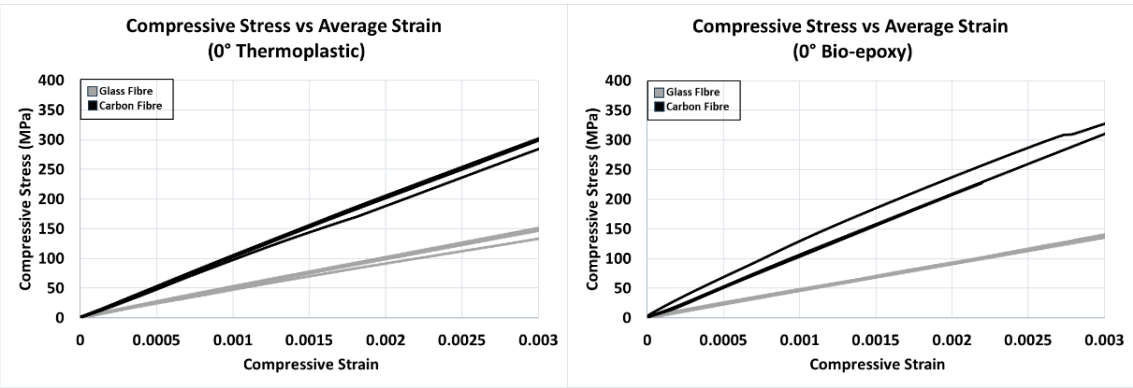

(a) (b)

Fig. 3. Stress-strain response curves for test coupons of 0° layup with (a) Thermoplastic (b) Bio-epoxy resin.

3.2 Failure Mechanisms

Fig. 4 and Fig. 5 depict the images of the tested specimens for GF and CF specimens, respectively. From Fig. 4(b) and 4(d) it can be observed that the 90° GF specimens primarily fail in the form of a crack aligned parallel to the primary fibre direction

(transverse to the loading) on a 45° shear plane. The CT scan observations confirm this failure mode. The post-compression test CT scans of GF specimens are presented in Fig. 6. In the case of 90° GF specimens (Fig. 6(c) and (d)), the y-z cross-section is shown at different locations ((iv), (v) and (vi)) across the width (x-direction) of the specimen. It is evident that the major failure mode is in the form of shear crack aligned at 45° to the loading direction (z-direction). Additionally, the x-y plane at different locations along the loading direction (z-direction), suggests some evidence of delamination in the shear crack zone (Fig. 6(c)ii and 6(d)ii). However, the scans indicate only a trace of damage at locations away from the shear crack. This indicates that the failure is localized near the crack region in 90° specimens. In the case of 0° specimens, visual inspection suggests the occurrence of multiple failure modes in the form of through-thickness shear, kinking or buckling. The CT scans provide further insight into the failure state of the specimens. From Fig. 6(a) (i) and 6 (b) (i) in x-y plane cross-sectional view, it can be observed that there are some cracks which travel across the thickness of the laminate, which indicate separation of fibres within the tows in the longitudinal direction. To further study this effect, the CT scans were inspected for each ply in 0° specimens and the obtained scans are presented in Fig. 7. Dark black lines allow the tows to be distinguished from one another. However, for the 1^{st} ply, specifically in the case of thermoplastic specimens (Fig. 7(a)), it can be seen that there are some longitudinal gaps present within a tow. Moreover, it appears that the angle with which the tows kink under compressive loading is slightly higher in 1^{st} and 4^{th} plies (exterior plies) than the 2^{nd} and 3^{rd} plies (internal plies). The internal plies are supported by adjacent plies. However, fibres in the external plies are only supported on one side. This makes fibres in the exterior plies more prone to buckling. Even though the failure modes are

different in 0° and 90° specimens, the visual and CT inspections do not suggest a particular influence on the overall failure modes due to the differing nature of the matrices within each of 0° and 90° specimens. However, the SEM observations reveal very distinctive characteristics at fibre-matrix interface level. This is discussed in detail in section 3.3.

In terms of failure mechanisms, SEM reveals further information. The images obtained from SEM are presented from Fig. 8 to Fig. 11. In the case of 0° GF specimens (Fig. 8(a) and Fig. 8(d)), there is evidence of matrix cracks resulting in separation of bundles of fibres from the bulk leading to their increased susceptibility to failure. This ultimately results in failure in the form of fibre fracture. The fractured surface of failed fibres can be seen in Fig. 8(c) and 8(f). The ultimate failure however involves a combination of different mechanisms. This can be seen more clearly in SEM images of CF specimens (Fig. 9(a) and 9(e)). Fig. 9(a) depicts one such failure site with evidence of fibre kinking along with fracture of fibres. Further, the fracture of groups of various fibres together as a bunch forms different fracture bands as evident from Fig. 9(a) and 9(d). Additionally, there is evidence of failure of the fibre-matrix interface due to less than optimum adhesion between fibres and matrix that can be clearly observed in Fig. 9(f) and 8(f) in the case of 0° Bio-epoxy specimens. This interface failure results in the formation of fibre imprints on the separated matrix. This is predominantly observed in Bio-epoxy based specimens and is less evident in thermoplastic based specimens, suggesting a stronger fibre-matrix adhesion in thermoplastic based specimens.

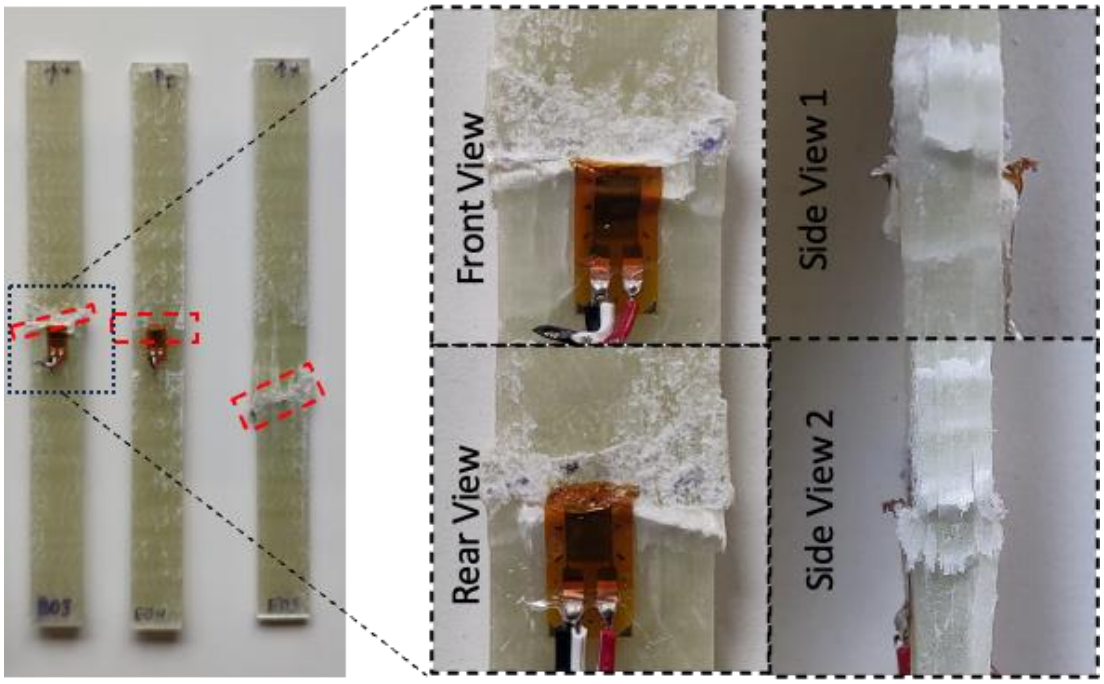
Front View
Side View 1
Rear View
Side View 2

(a)

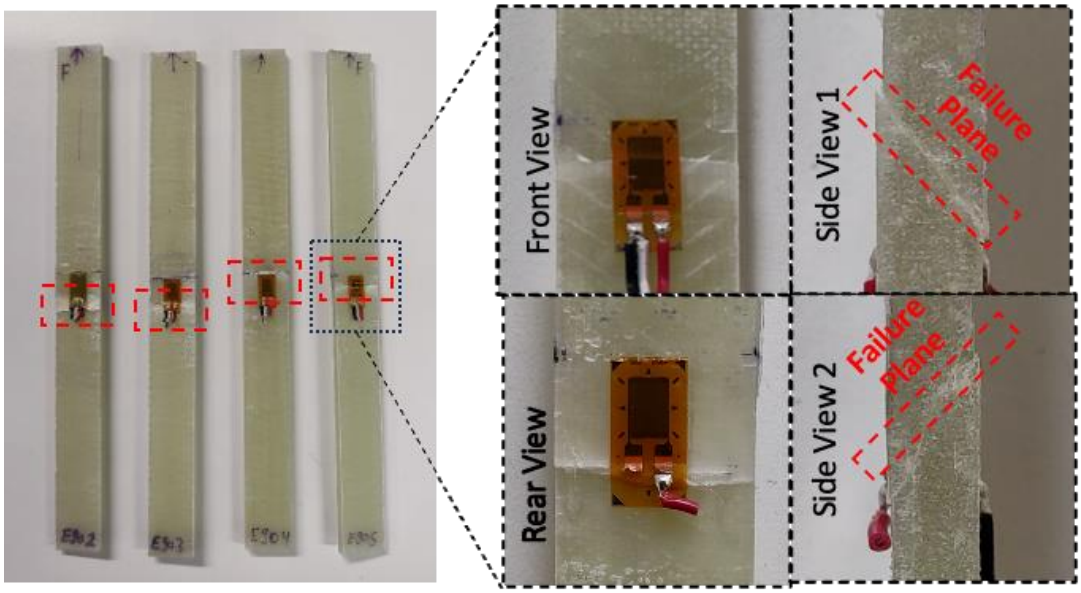
Front View
Side View 1
Failure Plane
Rear View
Side View 2
Failure Plane

(b)

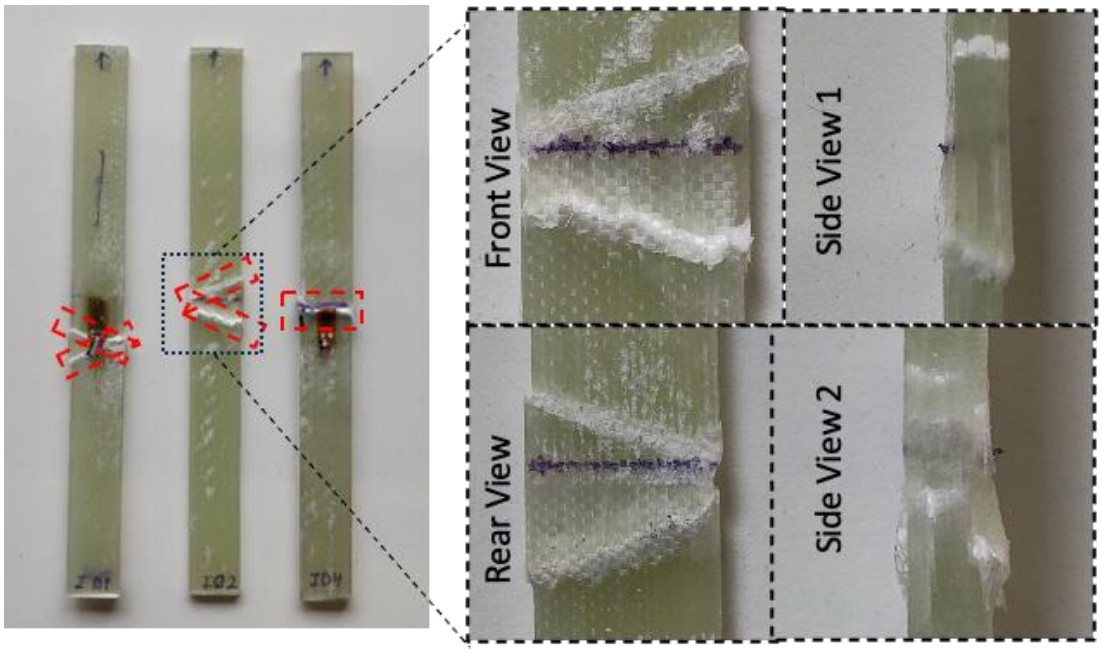

(c)

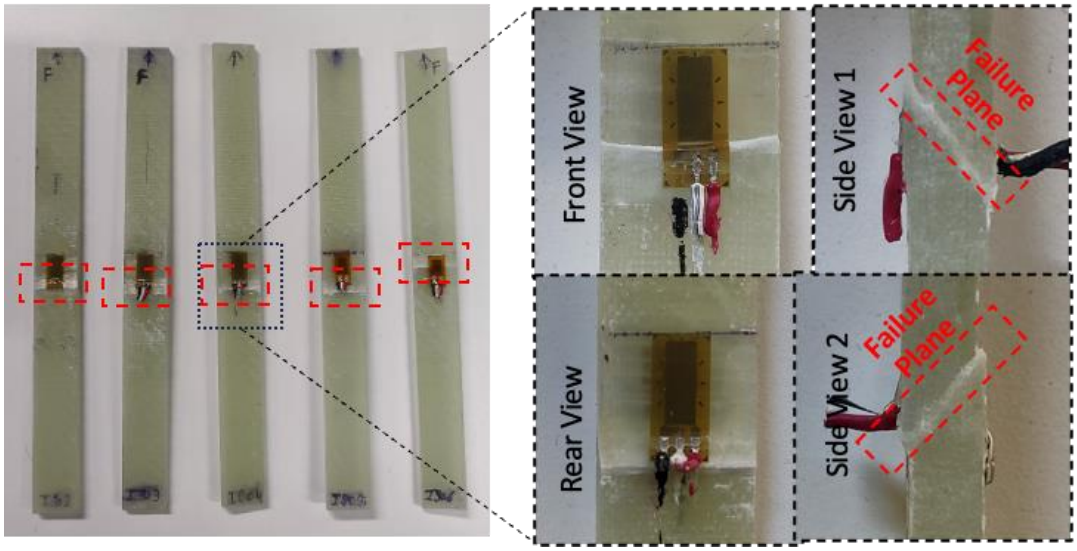

(d)

Fig. 4 Post testing specimen images depicting typical failure observed for glass-fibre reinforced (GF) specimens (a) GF/Thermoplastic 0° (b) GF/Thermoplastic 90° (c) GF/Bio-epoxy 0° (d) GF/Bio-epoxy 90° specimens.

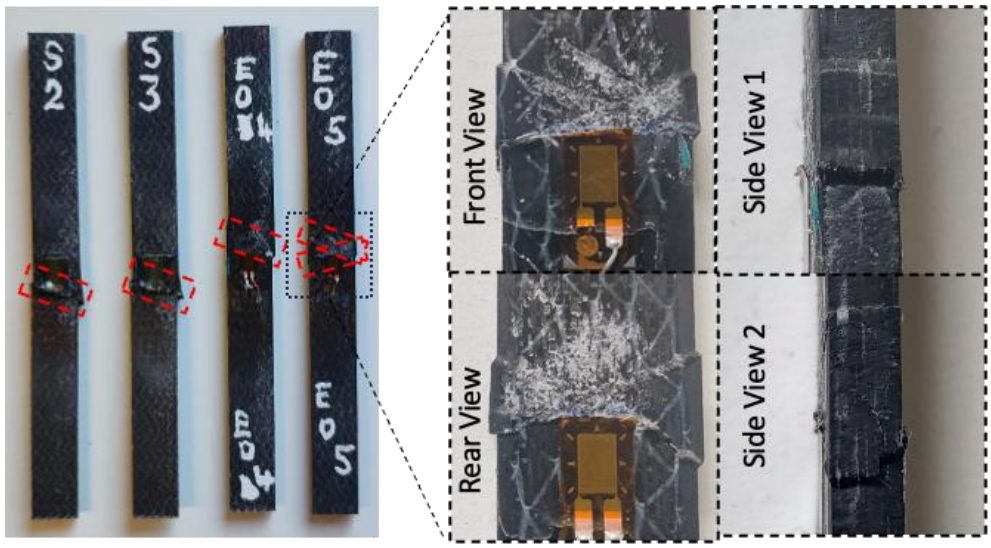
S2
S3
E04
E05
E04
E05
Front View
Side View 1
Rear View
Side View 2

(a)

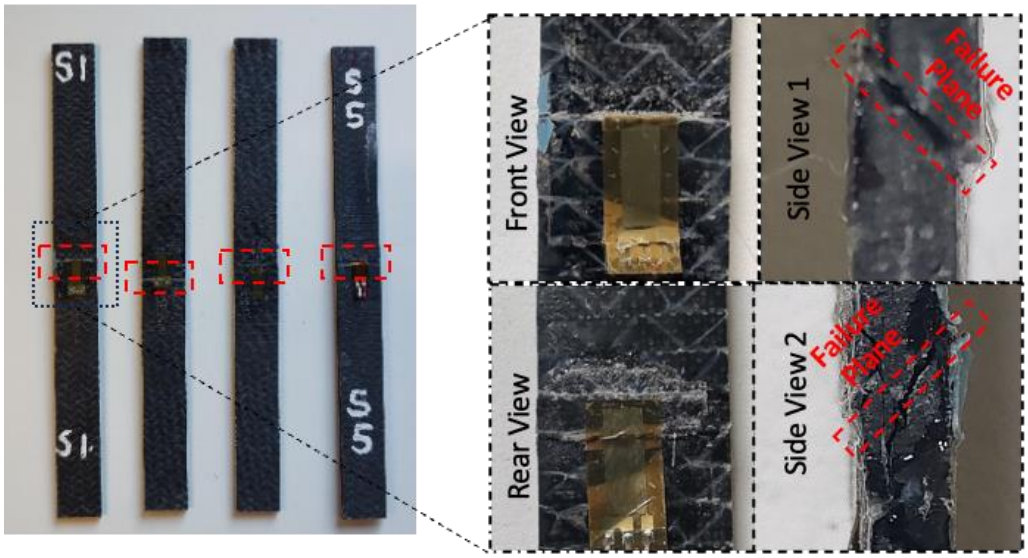
S1
S5
S1
S5
Front View
Side View 1
Failure Plane
Rear View
Side View 2
Failure Plane

(b)

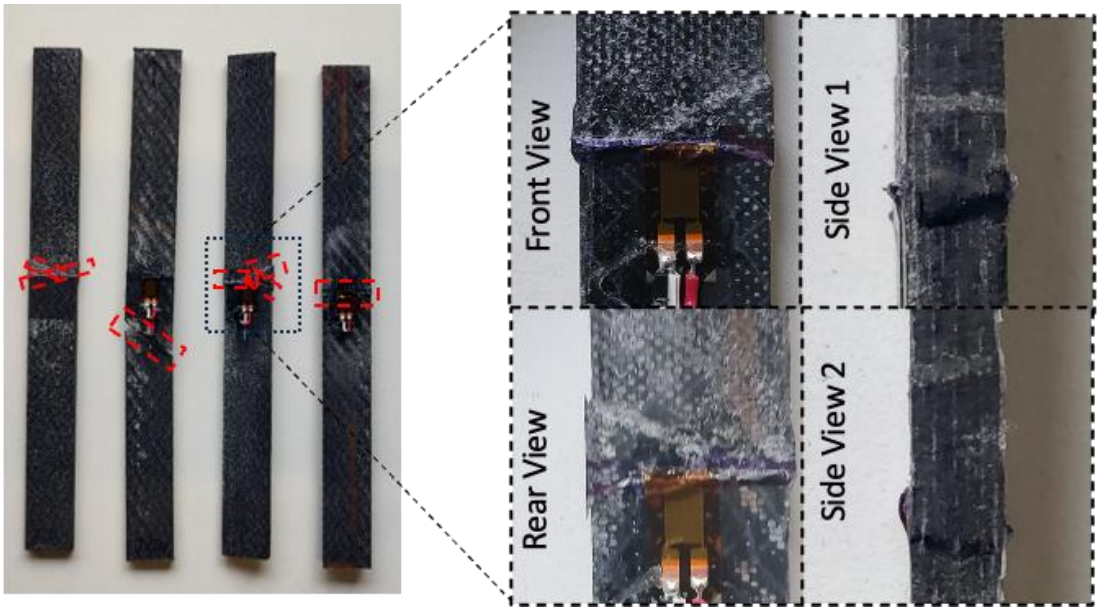

(c)

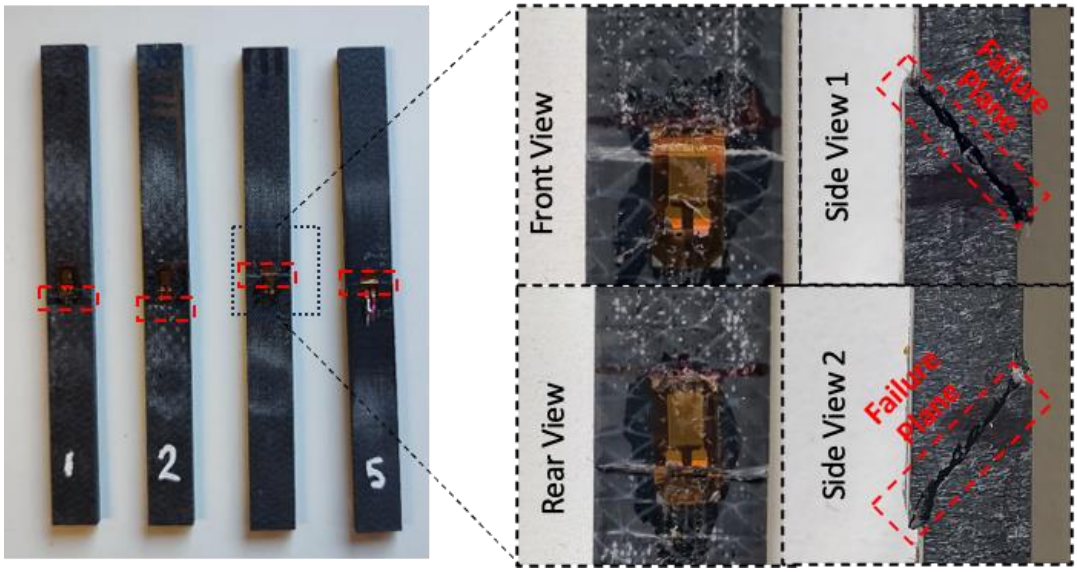

(d)

Fig. 5 Post testing specimen images depicting typical failure observed for carbon-fibre reinforced (CF) specimens (a) CF/Thermoplastic 0° (b) CF/Thermoplastic 90° (c) CF/Bio-epoxy 0° (d) CF/Bio-epoxy 90° specimens.

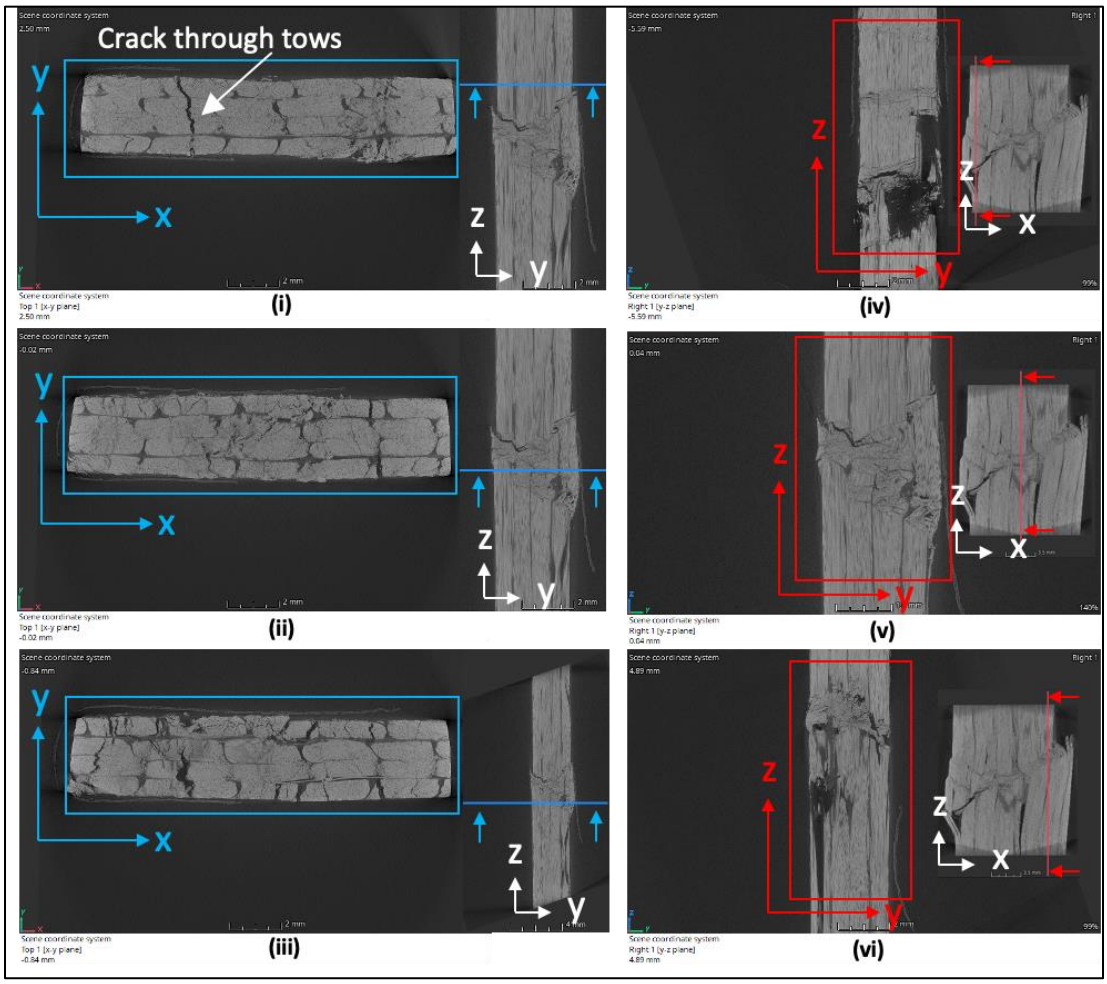

(a)

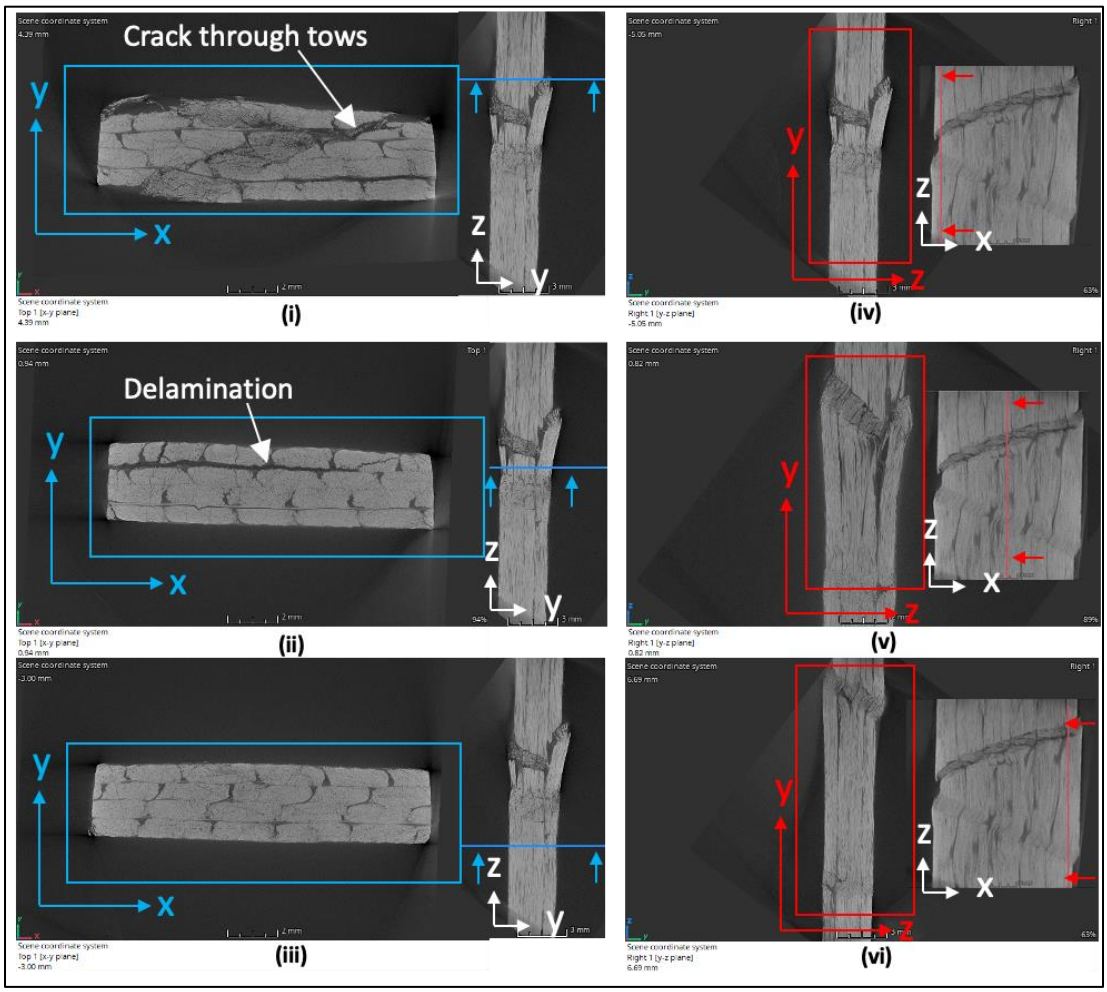

(b)

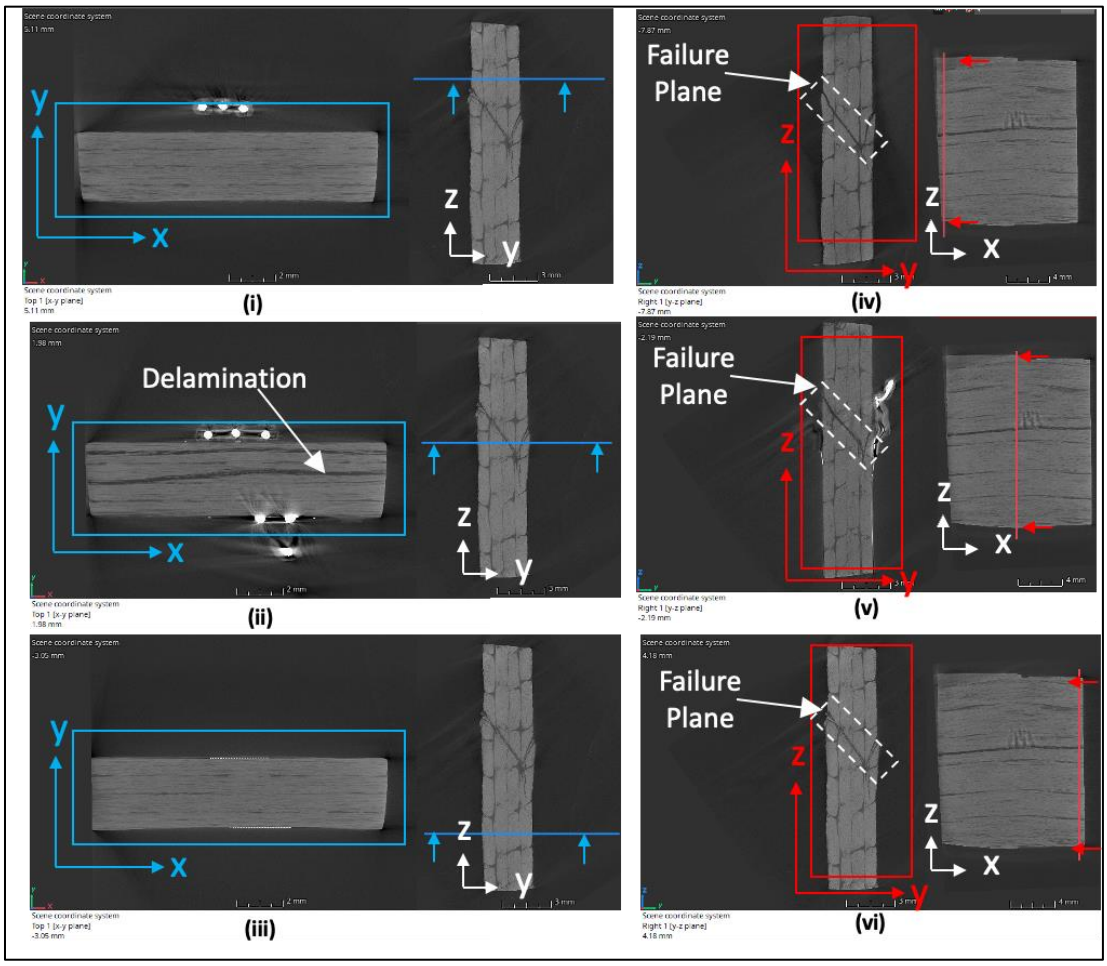
Failure Plane
Delamination
Failure Plane
Failure Plane
(i)
(ii)
(iii)
(iv)
(v)
(vi)

(c)

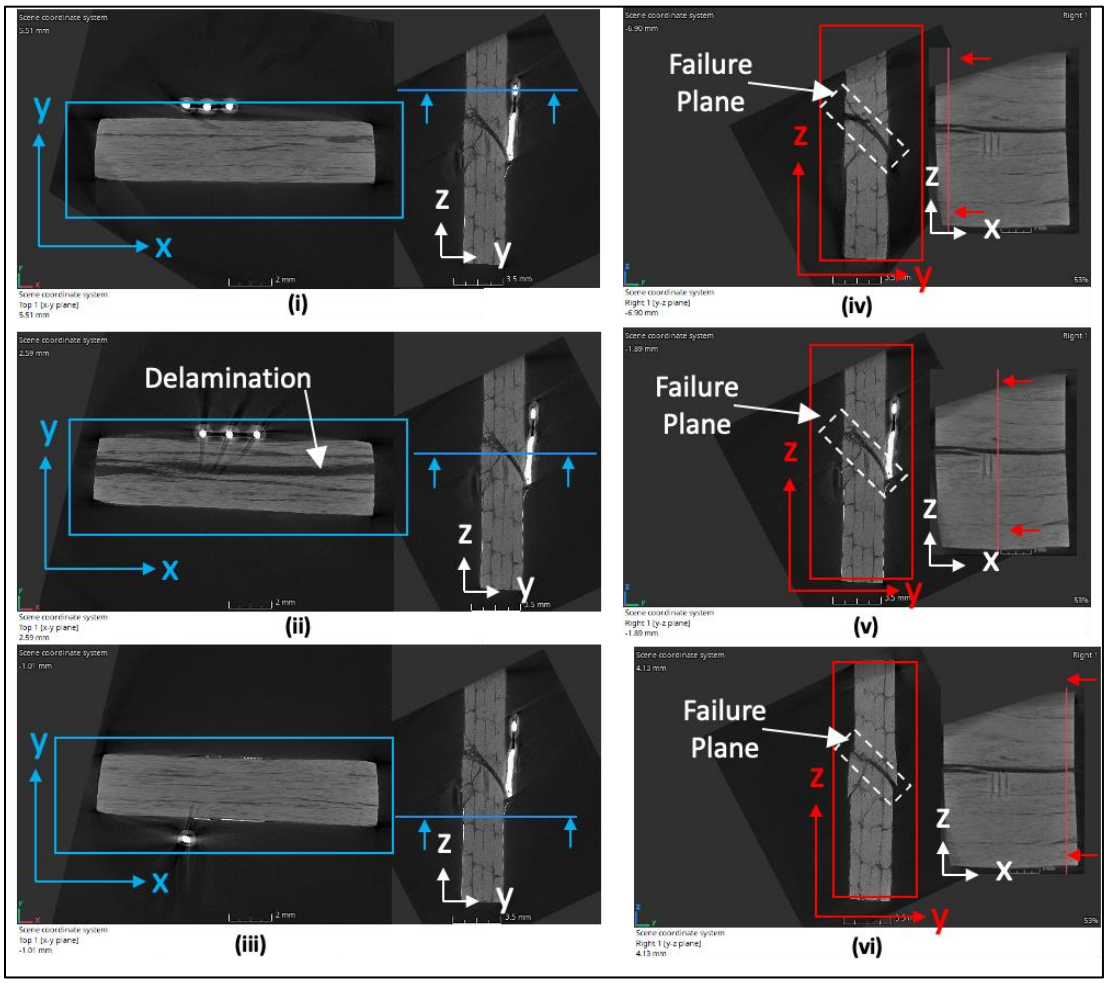

(d)

Fig. 6 Post testing CT scan images depicting typical failure mode observed near failure zone for glass-fibre reinforced (GF) specimens (a) GF/Thermoplastic 0° (b) GF/Bio-epoxy 0° (c) GF/Thermoplastic 90° (d) GF/Bio-epoxy 90° specimens. Note- Images (i), (ii) and (iii) depict cross-sectional view (x-y plane) at different locations across the height (z) of the specimen and Images (iv), (v) and (vi) depict cross-sectional view (y-z plane) at different locations across the width (x) of the specimens.

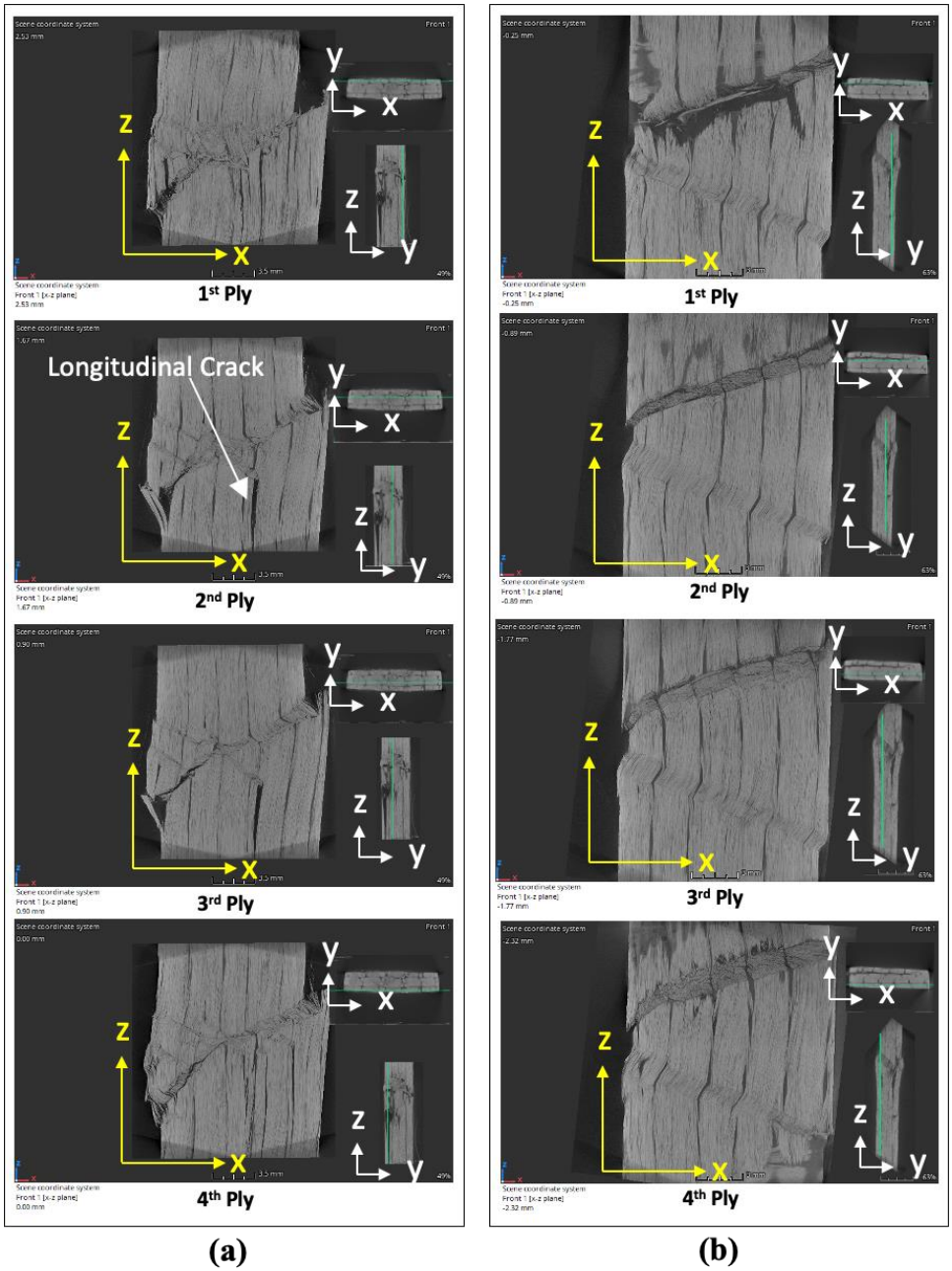

Fig. 7 Post testing CT scan images depicting typical failure observed in each ply (x-z plane) for glass-fibre reinforced (GF) specimens (a) GF/Thermoplastic 0° (b) GF/Bio-epoxy 0°

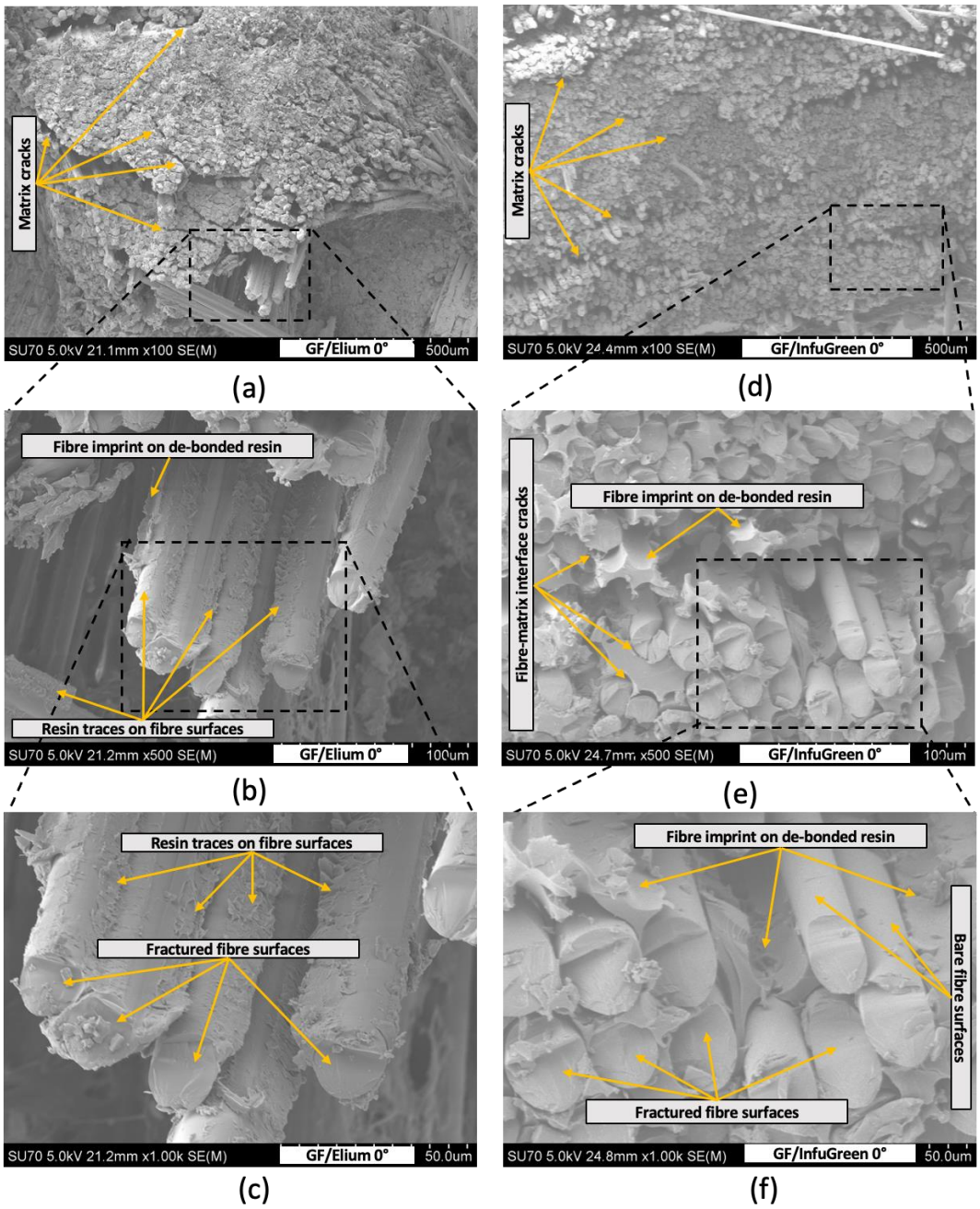

Fig. 8 SEM images depicting morphology of fractured surface in (a-c) GF/Thermoplastic 0° (d-f) GF/Bio-epoxy 0°.

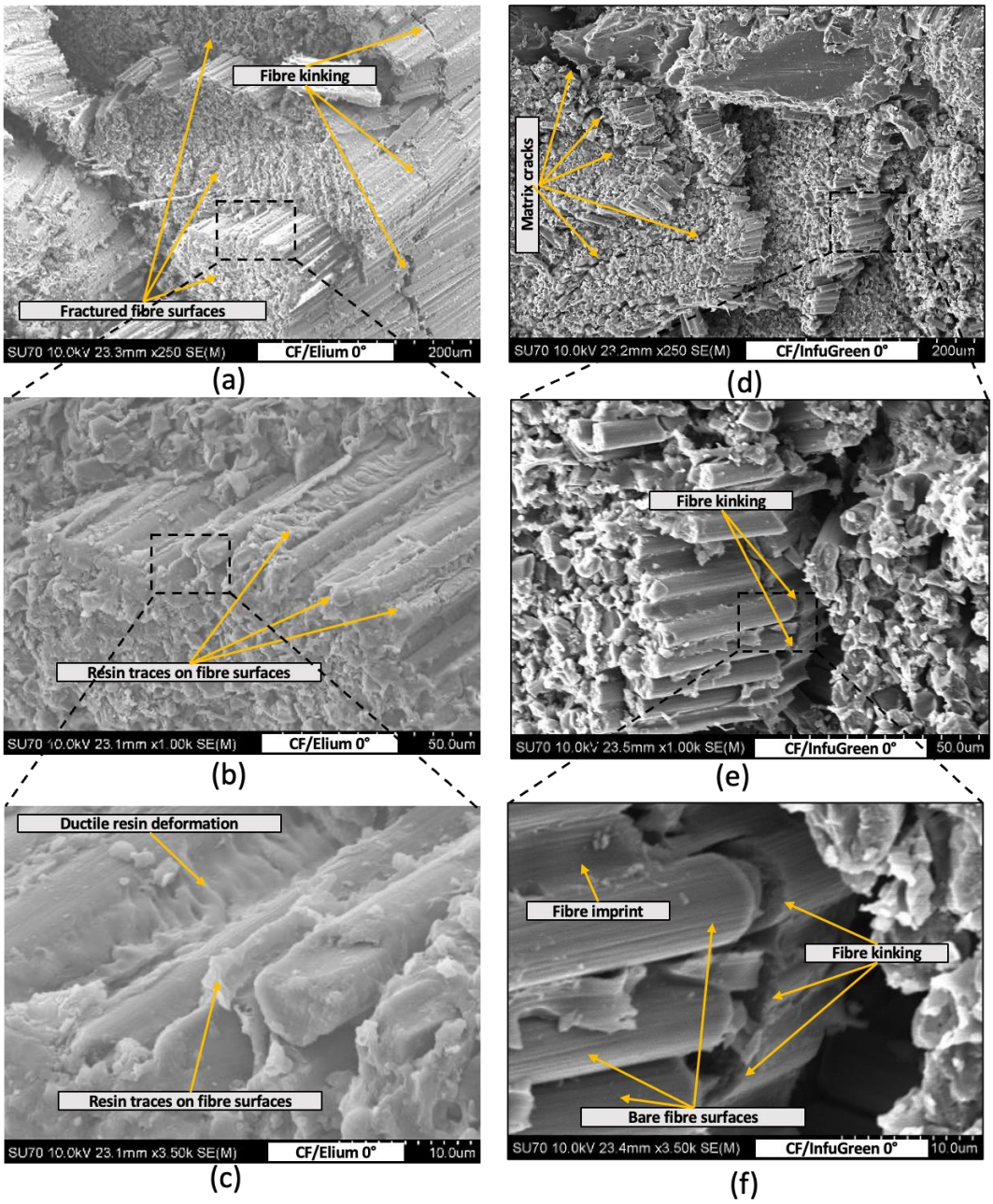

Fig. 9 SEM images depicting morphology of fractured surface in (a-c) CF/Thermoplastic 0° (d-f) CF/Bio-epoxy 0°

3.3 Matrix characteristics

A further analysis of the fracture surfaces under SEM indicates distinct fracture characteristics under compression for the bio-epoxy and thermoplastic matrix. A comparison of Fig. 10(c) and 10(f) reveals better adhesion of thermoplastic matrix to

carbon fibres compared with the bio-epoxy matrix. In the case of laminates employing the bio-epoxy matrix, the fibre surface is relatively cleaner, and the bare fibres are visible (Fig. 10(f)), whereas large traces of resin can be seen adhered to the fibres in the case of thermoplastic based specimens (Fig. 10(c)). A similar type of behaviour can be observed in the case of glass fibre-based laminates. As can be seen in Fig. 11(e) for GF/Bio-epoxy, the bare fibre surface is distinctively visible while in the case of GF/Thermoplastic laminates (Fig. 11(b)) the fibre surfaces are covered with resin. Furthermore, for 0° specimens as well, fibre surfaces were observed to exhibit similar characteristics. Fig. 8(c) and 9(c) show significant traces of thermoplastic resin on the fractured glass and carbon fibres whereas the fibre surfaces are relatively cleaner for GF/Bio-epoxy (Fig. 8(f)) and CF/Bio-epoxy (Fig. 9(f)) specimens. All these observations suggest a better adhesion characteristic of thermoplastic matrix compared to bio-epoxy for the specific fibre sizing employed.

Furthermore, the SEM images indicate that the thermoplastic based specimens with thermoplastic exhibit ductile characteristics while the specimens with bio-epoxy exhibit brittle attributes. From Fig. 10(b) and Fig. 11(c) it is observed that for the thermoplastic based laminates, the fracture surface consists of features such as microflow, risers, river lines which are distinct characteristics of a thermoplastic resin [17,29]. These observations can be attributed to the fact that the thermoplastic is likely to flow under compressive loading. On the other hand, the brittle characteristics of bio-epoxy are clear from Fig. 11(d)-11(f). It is observed that bio-epoxy tends to shatter in the form of small flakes at compressive failure. Hence it is inferred that both the resins have distinct characteristics under

compressive loading, with thermoplastic exhibiting typical plastic behaviour while bio-epoxy exhibiting typical brittle behaviour.

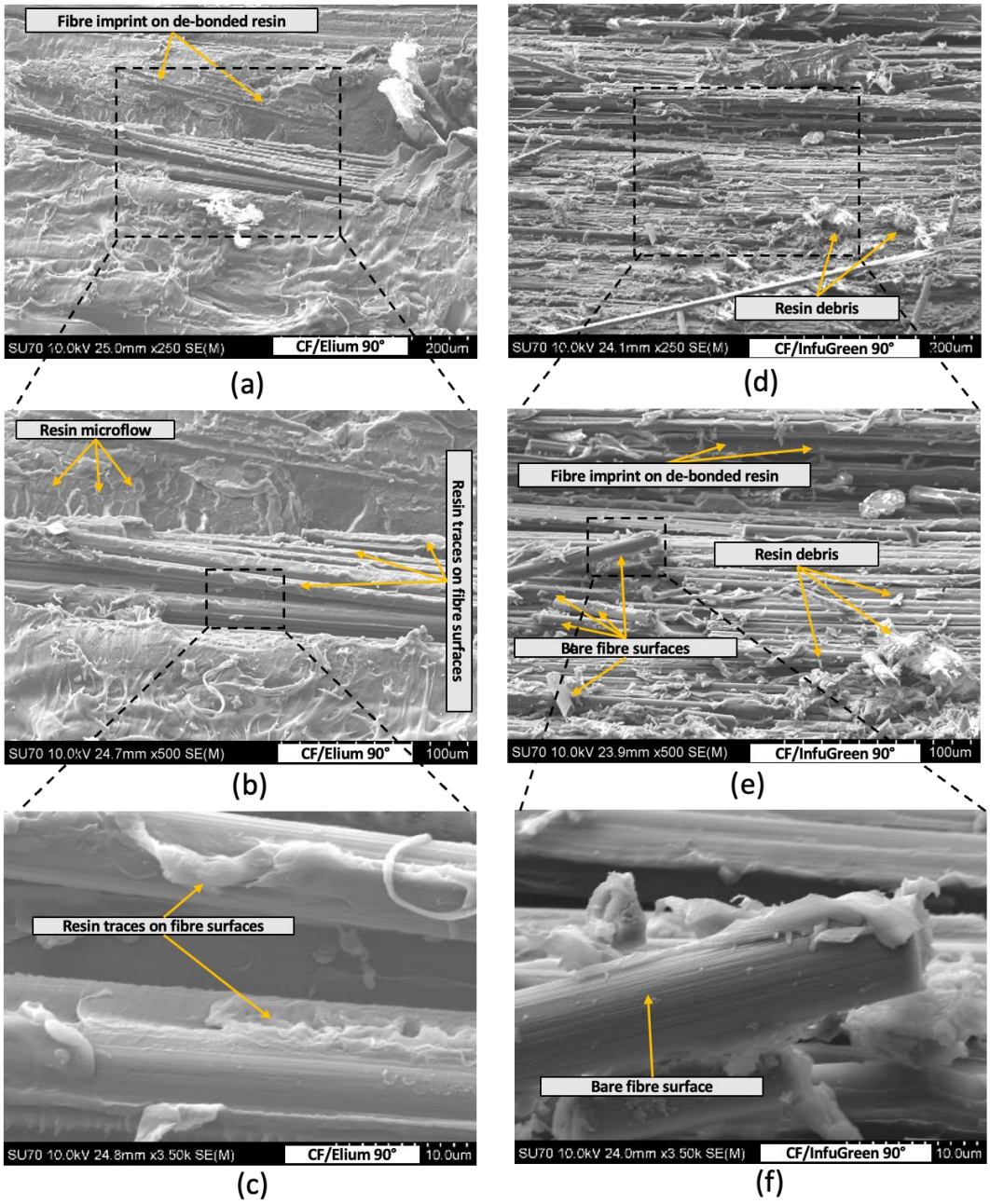

Fig. 10 SEM images depicting morphology of fractured surface in (a-c) CF/Thermoplastic 90° (d-f) CF/Bio-epoxy 90°

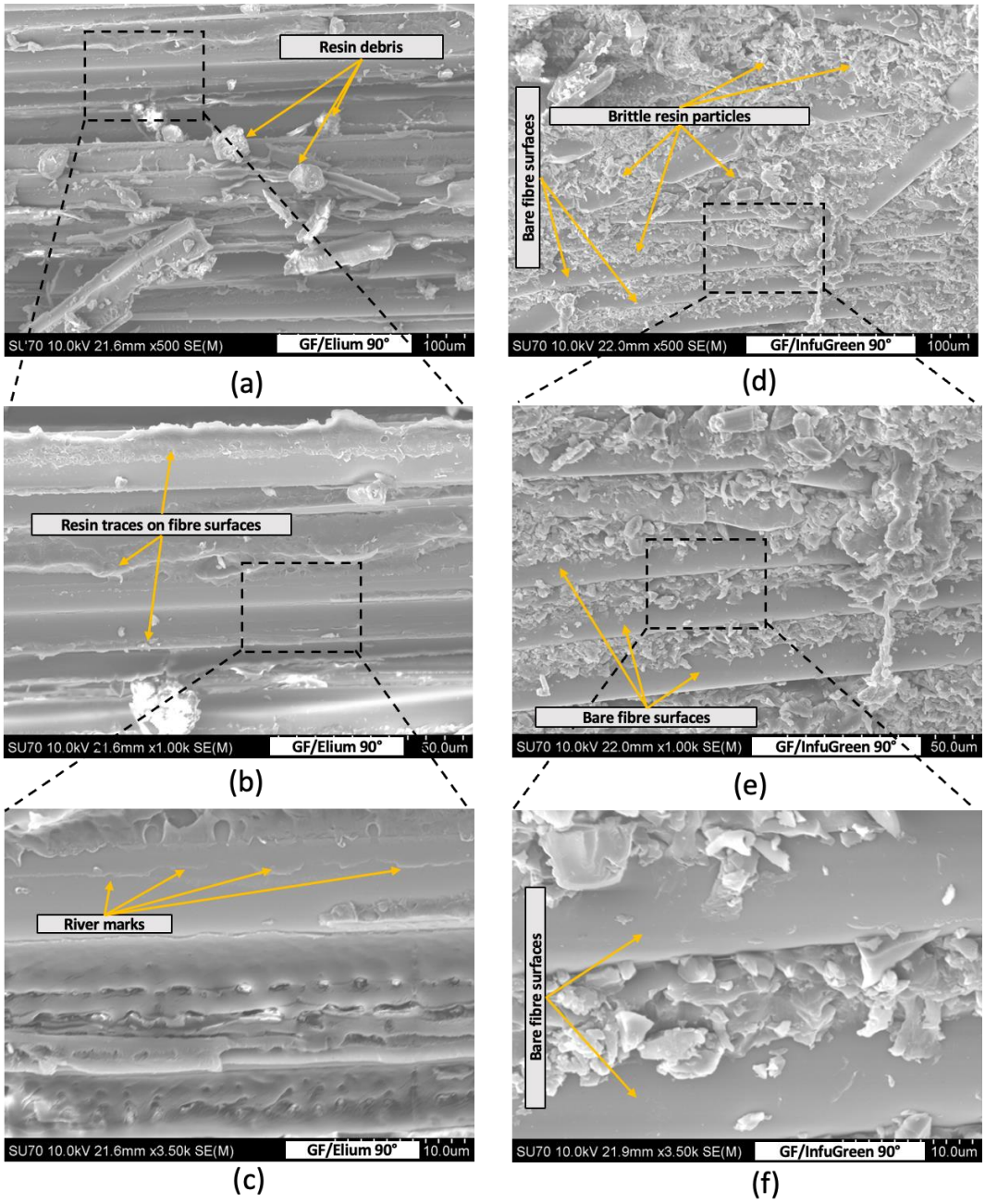

Fig. 11 SEM images depicting morphology of fractured surface in (a-c) GF/Thermoplastic 90° (d-f) GF/Bio-epoxy 90°

4. Conclusions

In this study, the compressive characterization results of composites comprising two different promising alternatives of petroleum-based epoxies viz. an in-situ polymerisable

thermoplastic (Elium®) and a bio-epoxy (InfuGreen®) reinforced with glass and carbon fibres are presented. The different failure modes are identified using visual inspection and computed tomography. Further, fractography analysis has been conducted using SEM which reveals distinctive characteristics for each resin system employed. From the characterized properties it is observed that for the same type of fibre reinforcement, thermoplastic based laminates have higher compressive strength compared to bio-epoxy based laminates. The fractography observations indicate better adhesion characteristic of thermoplastic matrix compared to bio-epoxy. Traces of thermoplastic matrix was present on fractured fibres while cleaner fractured fibre surfaces were observed for bio-epoxy based specimens for both glass and carbon fibre reinforcements. Thus, a stronger adhesion of thermoplastic to the reinforcement is leading to higher strength in the thermoplastic based specimens. In terms of the modulus exhibited by both thermoplastic and InfuGreen® based composites, it is observed that the performance of specimens for both matrix types was similar. From the modulus observations of 90° specimens, it is observed that the presence of a small amount (approx. 3 %) of reinforcement in the loading direction significantly increases the stiffness of the composite. Thus, fibre architecture plays a significant role in the stiffness offered by the laminate in the transverse loading under compression. From visual inspection and SEM observations, it is observed that a combination of various modes of failures (viz. kinking, buckling, shear cracking etc.) is present in the case of 0° specimens while failure in the form of transverse shear cracking in the matrix is predominantly observed in the case of 90° specimens. Thermoplastic matrix shows signs of plastic failure while bio-epoxy matrix shows brittle failure characteristics as is evident from post-test SEM images for 90° specimens. Overall, the composites

characterised have performed well in terms of compression strength and modulus under benign laboratory conditions using a manufacturing process relevant to large scale offshore structures. The two different resins studied, viz. bio resin and in-situ polymerizable thermoplastic provide options for manufacturers in terms of the sustainability strategy to be employed for the final structure. Future work must consider the effect of environment on these materials while the performance under fatigue loading is ongoing in a separate study.

Declaration of Competing Interest

The authors declare that they have no known competing financial interests or personal relationships that could have appeared to influence the work reported in this paper.

Acknowledgements

The authors would like to acknowledge that this work is funded under the European Union's Horizon 2020 research and innovation funding programme through the FIBREGY project (Grant Agreement Number 952966). The authors are thankful to the FIBREGY consortium partners for their valuable input and feedback on the work. The authors acknowledge the support received from Mr. Adrian McEvoy, University of Limerick towards mechanical testing. The authors are also thankful to the School of Engineering, University of Limerick, Ireland for providing access to test equipment and software.

Data Availability

The raw/processed data required to reproduce these findings cannot be shared at this time as the data forms part of an ongoing study.

References

[1] Bilgili M, Alphan H. Global growth in offshore wind turbine technology. Clean Technol Environ Policy 2022;24:2215–27. https://doi.org/10.1007/s10098-022-02314-0.
[2] Bilgili M, Alphan H, Ilhan A. Potential visibility, growth, and technological innovation in offshore wind turbines installed in Europe. Environmental Science and Pollution Research 2023;30:27208–26. https://doi.org/10.1007/s11356-022-24142-x.
[3] Soares-Ramos EPP, de Oliveira-Assis L, Sarrias-Mena R, Fernández-Ramírez LM. Current status and future trends of offshore wind power in Europe. Energy 2020;202:117787. https://doi.org/10.1016/j.energy.2020.117787.
[4] Adedipe O, Brennan F, Kolios A. Review of corrosion fatigue in offshore structures: Present status and challenges in the offshore wind sector. Renewable and Sustainable Energy Reviews 2016;61:141–54. https://doi.org/10.1016/j.rser.2016.02.017.
[5] Marsh G. Greater role for composites in wind energy. Reinforced Plastics 2014;58:20–4. https://doi.org/10.1016/S0034-3617(14)70037-2.
[6] Shamsuddoha M, Islam MM, Aravinthan T, Manalo A, Lau K tak. Effectiveness of using fibre-reinforced polymer composites for underwater steel pipeline repairs. Compos Struct 2013;100:40–54. https://doi.org/10.1016/j.compstruct.2012.12.019.
[7] Liu P, Barlow CY. Wind turbine blade waste in 2050. Waste Management 2017;62:229–40. https://doi.org/10.1016/j.wasman.2017.02.007.
[8] Lefeuvre A, Garnier S, Jacquemin L, Pillain B, Sonnemann G. Anticipating in-use stocks of carbon fibre reinforced polymers and related waste generated by the wind power sector until 2050. Resour Conserv Recycl 2019;141:30–9. https://doi.org/10.1016/j.resconrec.2018.10.008.
[9] Zhao X, Long Y, Xu S, Liu X, Chen L, Wang YZ. Recovery of epoxy thermosets and their composites. Materials Today 2023. https://doi.org/10.1016/j.mattod.2022.12.005.
[10] Bernatas R, Dagreou S, Despax-Ferreres A, Barasinski A. Recycling of fiber reinforced composites with a focus on thermoplastic composites. Clean Eng Technol 2021;5. https://doi.org/10.1016/j.clet.2021.100272.
[11] Cousins DS, Suzuki Y, Murray RE, Samaniuk JR, Stebner AP. Recycling glass fiber thermoplastic composites from wind turbine blades. J Clean Prod 2019;209:1252–63. https://doi.org/10.1016/j.jclepro.2018.10.286.
[12] Van Rijswijk K, Bersee HEN. Reactive processing of textile fiber-reinforced thermoplastic composites - An overview. Compos Part A Appl Sci Manuf 2007;38:666–81. https://doi.org/10.1016/j.compositesa.2006.05.007.
[13] ZEBRA project achieves key milestone with production of the first prototype of its recyclable wind turbine blade March 17, 2022 n.d. https://www.ge.com/news/press-releases/zebra-project-achieves-key-milestone-with-production-of-first-prototype-of-recyclable-wind-turbine-blade (accessed July 19, 2023).
[14] Terry JS, Taylor AC. The properties and suitability of commercial bio-based epoxies for use in fiber-reinforced composites. J Appl Polym Sci 2021;138:1–12. https://doi.org/10.1002/app.50417.

[15] Haggui M, El Mahi A, Jendli Z, Akrout A, Haddar M. Static and fatigue characterization of flax fiber reinforced thermoplastic composites by acoustic emission. Applied Acoustics 2019;147:100–10. https://doi.org/10.1016/j.apacoust.2018.03.011.
[16] Barbosa LCM, Bortoluzzi DB, Ancelotti AC. Analysis of fracture toughness in mode II and fractographic study of composites based on Elium® 150 thermoplastic matrix. Compos B Eng 2019;175. https://doi.org/10.1016/j.compositesb.2019.107082.
[17] Kazemi ME, Shanmugam L, Lu D, Wang X, Wang B, Yang J. Mechanical properties and failure modes of hybrid fiber reinforced polymer composites with a novel liquid thermoplastic resin, Elium®. Compos Part A Appl Sci Manuf 2019;125:105523. https://doi.org/10.1016/j.compositesa.2019.105523.
[18] Pini T, Briatico-Vangosa F, Frassine R, Rink M. Matrix toughness transfer and fibre bridging laws in acrylic resin based CF composites. Eng Fract Mech 2018;203:115–25. https://doi.org/10.1016/j.engfracmech.2018.03.026.
[19] Pini T, Caimmi F, Briatico-Vangosa F, Frassine R, Rink M. Fracture initiation and propagation in unidirectional CF composites based on thermoplastic acrylic resins. Eng Fract Mech 2017;184:51–8. https://doi.org/10.1016/j.engfracmech.2017.08.023.
[20] Obande W, Mamalis D, Ray D, Yang L, Ó Brádaigh CM. Mechanical and thermomechanical characterisation of vacuum-infused thermoplastic- and thermoset-based composites. Mater Des 2019;175:107828. https://doi.org/10.1016/j.matdes.2019.107828.
[21] Nash NH, Portela A, Bachour-Sirerol CI, Manolakis I, Comer AJ. Effect of environmental conditioning on the properties of thermosetting- and thermoplastic-matrix composite materials by resin infusion for marine applications. Compos B Eng 2019;177:107271. https://doi.org/10.1016/j.compositesb.2019.107271.
[22] Jia Y, Fiedler B. Tensile creep behaviour of unidirectional flax fibre reinforced bio-based epoxy composites. Composites Communications 2020;18:5–12. https://doi.org/10.1016/j.coco.2019.12.010.
[23] Liu Z, Wang H, Yang L, Du J. Research on mechanical properties and durability of flax/glass fiber bio-hybrid FRP composites laminates. Compos Struct 2022;290:115566. https://doi.org/10.1016/j.compstruct.2022.115566.
[24] Le Duigou A, Davies P, Baley C. Seawater ageing of flax/poly(lactic acid) biocomposites. Polym Degrad Stab 2009;94:1151–62. https://doi.org/10.1016/j.polymdegradstab.2009.03.025.
[25] Lu MM, Fuentes CA, Van Vuure AW. Moisture sorption and swelling of flax fibre and flax fibre composites. Compos B Eng 2022;231. https://doi.org/10.1016/j.compositesb.2021.109538.
[26] Reimer V, Dyagilev AS, Liebenstund L, Kuznetsov AA, Gries T. Estimation of Strength of Composites Reinforced with Woven Preform. Fibre Chemistry 2019;50:538–42. https://doi.org/10.1007/s10692-019-10025-4.
[27] Datasheet T. ELIUM ® 188 O LIQUID THERMOPLASTIC RESIN TYPICAL CURED RESIN NON REINFORCED PROPERTIES; URL: ; URL: https://www.arkema.com/files/live/sites/shared_arkema/files/downloads/products-documentations/liquid-thermoplastic-resinfor-tougher-composites.pdf. n.d.

[28] Datasheet T. ELIUM ® 188 XO LIQUID THERMOPLASTIC RESIN TYPICAL CURED RESIN NON REINFORCED PROPERTIES; URL: https://www.arkema.com/files/live/sites/shared_arkema/files/downloads/products-documentations/liquid-thermoplastic-resinfor-tougher-composites.pdf. n.d.
[29] ASTM. Standard Test Method for Compressive Properties of Polymer Matrix Composite Materials Using a Combined Loading Compression (CLC). Annual Book of ASTM Standards 2012;i:1–11. https://doi.org/10.1520/D6641.
[30] Global SAI, Iso F, License C, Global SAI. ISO 14127 Carbon-fibre-reinforced composites — Determination of the resin, fibre and void contents. International Standard 2015;44.
[31] Bhudolia SK, Gohel G, Vasudevan D, Leong KF, Gerard P. Delamination behaviour and surface morphology of wholly thermoplastic composites using different ultra-high molecular weight thermoplastic fabrics with pristine and toughened Elium resin under Mode I loading. Compos Part A Appl Sci Manuf 2023;164. https://doi.org/10.1016/j.compositesa.2022.107273.